

# Fe-Cu binary oxides as low-cost adsorbents and their application to photocatalytic removal of Acid Red 14, Methyl Orange, and Malachite Green from aqueous solutions

Seyyed Hamed Zafari,<sup>a</sup> Naghi Saadatjou,<sup>\*a</sup> and Behrouz Shaabani<sup>\*b</sup>

<sup>a</sup> Department of Applied Chemistry, Faculty of Chemistry, Semnan University, Semnan, Iran

<sup>b</sup> Department of Inorganic Chemistry, Faculty of Chemistry, University of Tabriz, Tabriz, Iran

Article history:

Received: 03/ Feb /2020

Received in revised form: 22/Jul/2020

Accepted: 22/Jul/2020

## Abstract

In this work, a series of binary oxides with 0:1, 1:10, 1:7, 1:5, and 1:0 CuFe molar ratios were synthesized by a simple, low cost, and effective procedure. The anionic dyes, namely Acid Red 14 (AR14), Methyl Orange (MO), and Malachite Green (MG) as a cationic dye removal and adsorption onto these materials was investigated. The effects of Cu:Fe molar ratio, pH, and sorbent dosage were investigated at 25±1 °C. The synthesized adsorbent compound containing 1:7 molar ratio of Cu:Fe verified to possess an uppermost dye adsorption capacity. Subsequently, this new sorbent was characterized by different techniques such as Fourier transform infrared spectroscopy (FT-IR), X-ray powder diffraction (XRD), Scanning electron microscopy (SEM), Transmission electron microscopy (TEM), and Energy-dispersive X-ray spectroscopy (EDX). The new nanostructure was confirmed for dye adsorption in the presence of UV irradiation. Selected Fe-Cu binary oxide exposed the highest adsorption capacities of MG as compared with the other dyes. It would be a practical process to remove MG from aqueous solution by increasing adsorption efficacy during wastewater treatment. The photocatalytic performance of the as-fabricated binary oxides was surveyed with the destruction of dye.

**Keywords:** Fe-Cu binary oxides; Dye adsorption; Acid Red 14; Methyl Orange; Malachite Green.

## 1. Introduction:

Manufacturers widely employ dyes and pigments to color their versatile products. Several criteria, such as chemical structure, solubility, and different application technologies, lead to the diversity of dyes [1, 2].

They can be classified by their method of application to the substrate. Such a classification would include anionic (direct, acid, and reactive dyes), cationic (basic dyes), and non-ionic (disperse dyes) [3, 4].

\*.Corresponding author: Associate Professor of Inorganic Chemistry, Department of Inorganic Chemistry, Faculty of Chemistry, University of Tabriz, Tabriz, Iran. E-mail Address: shaabani.b@gmail.com  
Professor of Applied Chemistry, Department of Chemistry, Faculty of Chemistry, Semnan University, Semnan, Iran. E-mail Address: naghisjo@gmail.com

Before releasing industrial wastewater into the environment and natural water streams, we need to exploit advanced and effective techniques to eliminate hazardous dyes from industrial wastes. A variety of treatment fields, including biodegradation with fungi [3], coagulation process [5, 6], oxidation reaction [7, 8], nanofiltration [9], and adsorption [4, 10, 11] have been employed for the removal of dye-containing effluents. In case the simplicity of a design and cost-effective approach for large scale production with an adsorption method has been proved, adsorption methods would be known as a notable method in dye removal technologies [12]. Therefore, developing effective adsorbents for wastewater treatment is desirable and also a versatile platform for the removal of toxic dye pollutants.

The nano-sized materials are often composed of metal oxides or metals, with the particle size that is changing between 1nm and 50 nm. The enthusiasm about the metal oxide nanoparticles has grown over the last few decades due to their robust, readily available, high surface area, high dispersion, and high stability properties [12-14]. Numerous types of metal oxide sorbents have been successively researched in the field of dye degradation, and, among them, iron oxides are quite promising candidates for their high affinity to dyes [15-19].

Zinatloo et al., successfully synthesized novel  $Dy_2Sn_2O_7$  nanostructures with *Ficus carica* and used it as visible-light-sensitive photocatalyst for the destruction of Acid Violet 7 and crystal violet and also removal and destruction of organic contaminants in water [20]. Zinatloo et al., successfully synthesized  $Ho_2O_3$  [21] and  $Dy_2Ce_2O_7$  [22], [22], and [20], and investigated their photocatalyst activity. Recently, the exploitation of composite sorbents that hold two or more metal oxides draws a significant amount of focus in the field of adsorption techniques, and numerous studies address the use of binary oxides such as Nd-Sn [22],

Fe-Ce [23], Fe-Mn [24], Fe-Ti [25], Fe-Ni [26], Fe-Al, Fe-Zr [27], etc. The incorporation of other polyvalent metal ions into iron oxide nanoparticles gives rise to a strong increase in adsorption capacity. Since the adsorption capacity of the copper oxide nanoparticles is less examined [28, 29], our investigation will focus on the mentioned nanoaterials. Thus, we will incorporate copper into the lattice structure of iron oxide to design a Fe-Cu binary oxide adsorbent compound. Bimetallic adsorbents tend to demonstrate improved adsorption performance over industrial dyes as compared with pure oxides. As we all know, there are only a few papers regarding the synthesis of Fe-Cu binary oxide and its unique properties as a low-cost adsorbent. In this regard, Zhang et al., [30] reported that their synthesized adsorbent compound containing 1:2 molar ratio of Cu:Fe had an exceptional performance in removing arsenic from water and claimed that the highest adsorption capacities for As(III) and As(V) at a pH of 7.0 were 122.3 and 82.7 mg/g, respectively. Also, they developed the Fe-Cu binary oxide adsorbent and showed higher phosphate adsorption [31]. Yuanfeng et al., in 2018 synthesized the  $Fe_3O_4@SiO_2@Fe_2O_3-CuO/TiO_2$  (Mag@Fe-Cu/TiO<sub>2</sub>) adsorbent, and the synthesized adsorbent compound showed good reusability for arsenic removal by the oxidation of As(III). Tofik[32] synthesized the Fe-Al oxide sorbent for phosphate sorption. Li et al., prepared iron-copper binary oxide and investigated the effect of its removal from the water on antimony (V) [33]. Jacukowicz-Sobala synthesized Cu (II)-Fe (III) oxide doped anion exchangers as multifunctional composites for arsenite removal from water via As (III) adsorption and oxidation [34].

The present study demonstrates the synthesis of Fe-Cu binary oxides at room temperature for the simultaneous adsorption and photocatalytic removal

of various dye pollutants from aqueous solutions by UV light irradiation.

## **2. Experimental:**

### **2.1. Materials and methods**

All chemicals used in this study were analytical reagent grade. Iron(III) chloride hexahydrate( $\geq 98\%$ ) and Copper(II) sulfate pentahydrate( $\geq 98\%$ ) were purchased from Sigma-Aldrich. The Fe-Cu particles were characterized by the following methods. The micrographs of the materials were detected by a 30 kV HITACHI S-3000N scanning electron microscopy (SEM). Transmission electron microscopy (TEM) was carried out on a JEM-200CX. FT-IR spectra of the samples were recorded in KBr wafers by SHIMADZU 8201PC, FT-IR spectrophotometer. The X-ray diffraction (XRD) patterns of the mixed oxide were recorded at room temperature by X-ray diffractometer (JEOLJDX-3532).

### **2.2. Preparation of Fe-Cu bimetal oxide adsorbents**

A reported co-precipitation method was adopted for the preparation of a series of Fe-Cu binary oxides with 0:1, 1:10, 1:7, 1:5, and 1:0 Cu:Fe molar ratios at room temperature [30]. The precise amounts of  $\text{FeCl}_3 \cdot 6\text{H}_2\text{O}$  and  $\text{CuSO}_4 \cdot 5\text{H}_2\text{O}$ , as raw materials, were mixed in 400 ml deionized water and stirred vigorously. According to the required Cu:Fe molar ratio, the amount of  $\text{CuSO}_4 \cdot 5\text{H}_2\text{O}$  or  $\text{FeCl}_3 \cdot 6\text{H}_2\text{O}$  was adjusted to the predetermined value. Under this condition, the sodium hydroxide solution (3 M) was added dropwise until the pH of the liquid approximately rose to 7.5, and the stirring was continued more than 15 min. The emerged suspension was allowed to stand for two days in the solution state without disturbing. After the decantation of the liquid from the obtained precipitate, the suspension was washed three times with distilled water and then filtered and later dried at 60 °C for 24 h.

### **2.3. Dye solutions**

In a 100 mL volumetric flask full of double-distilled water, we dissolved a specific amount of dye. The dye solution of the wanted concentration for working was made by dilution of a measured volume of this stock with double distilled water. The stock was prepared again in every time interval. After that, UV-vis spectroscopy measurements were used for the calculation of the concentration of each experiment.

### **2.4. Dye photocatalytic sorption procedure**

Based on the batch equilibrium technique [3], the substantial purpose was to attain an appropriate model that could make a valid prediction on the percentage of various dye removals from aqueous solution onto bimetal oxide adsorbents. Here, 50 mL of dye solution with a specific concentration was taken with 15 mg photocatalyst in 1000 mL glass vessel and placed inside a reactor equipped with a rotator and UV lamp (6 W, 254 nm maximum emission). The suspension was mixed with 120 rpm and 25 °C for 3 h at an equilibrium pH of 7.0. The pH of the solutions was adjusted by 0.1 M HCl and/or 0.1 M NaOH solutions as required. The samples were taken and allowed to settle by a centrifuging machine with 3000 rpm at different intervals of time. By using a UV-vis spectrophotometer for the concentration of residual dye, we separated the solutions of the specified samples from the sorbent material and analyzed them.

## **3. Results and discussion**

### **3.1. Characterization of Fe-Cu bimetal oxide as adsorbents**

The Fe-Cu bi-metal oxide with a Cu:Fe molar ratio of 1:7, as a new bimetallic oxide, was characterized by Fourier transform infrared spectroscopy (FTIR), X-ray diffraction (XRD), scanning electron microscopy (SEM), and energy-dispersive X-ray spectroscopy (EDX).

The FT-IR spectrum (see Fig. 1) exhibits a wide-stretching vibration in the range of 3200-3600  $\text{cm}^{-1}$ , which is an indicator of the presence of the -OH groups in the products. Besides, vibration bands observed at around 400-700  $\text{cm}^{-1}$  are due to the vibration modes of Fe-O and Cu-O bonds and confirm the formation of Cu-Fe binary oxide. The two-weak peaks at 943.7 and 1074.6  $\text{cm}^{-1}$  are related to the vibration of  $\text{SO}_4^{2-}$ . The observation of the spectrum suggests the presence of adsorbed

carbonate ions of the atmosphere, and it was verified by the characteristic stretching band at 1358  $\text{cm}^{-1}$ . Also, the presence of a vibration band with medium intensity in 1636.5  $\text{cm}^{-1}$  is allocated to the deformation of water molecules. That showed the existence of physisorbed water on the oxide [31, 35]. In Table 1, we compare our synthetic binary oxide with a previous paper about binary oxide photocatalyst activity.

**Table 1.** A comparison of synthetic binary oxide with previous paper.

Compound	Remove	ref
Fe/Cu	Sb(V)	[33]
CuFeO <sub>2</sub> and CuO binary films	visible photocatalytic activity	[21]
Fe-Al binary oxide	99.86% phosphate adsorption	[32]
Al <sub>2</sub> O <sub>3</sub> -Nd <sub>2</sub> O <sub>3</sub> Binary Oxides	Diclofenac	[36]
GNPs/Ti-Fe binary oxide	photocatalytic performance in visible light	[37]
Fe <sub>2</sub> O <sub>3</sub> /Cu <sub>2</sub> O nanocomposite	visible-light photocatalytic activity for the degradation of cationic dyes	[38]
$\alpha$ -Fe <sub>2</sub> O <sub>3</sub> /Cu <sub>2</sub> O mixed oxide	visible light photocatalytic activity	[39]
Zn-Fe mixed metal oxides	removal of several pharmaceuticals and arsenic	[40]
Graphitized carbon-coated bimetallic FeCu nanoparticles	improving photocatalytic activity	[41]
ZnTiO <sub>3</sub> -TiO <sub>2</sub>	photocatalytic activity under solar light irradiation	[42]
Fe-Mn binary oxide	Adsorption of methylene blue	[43]

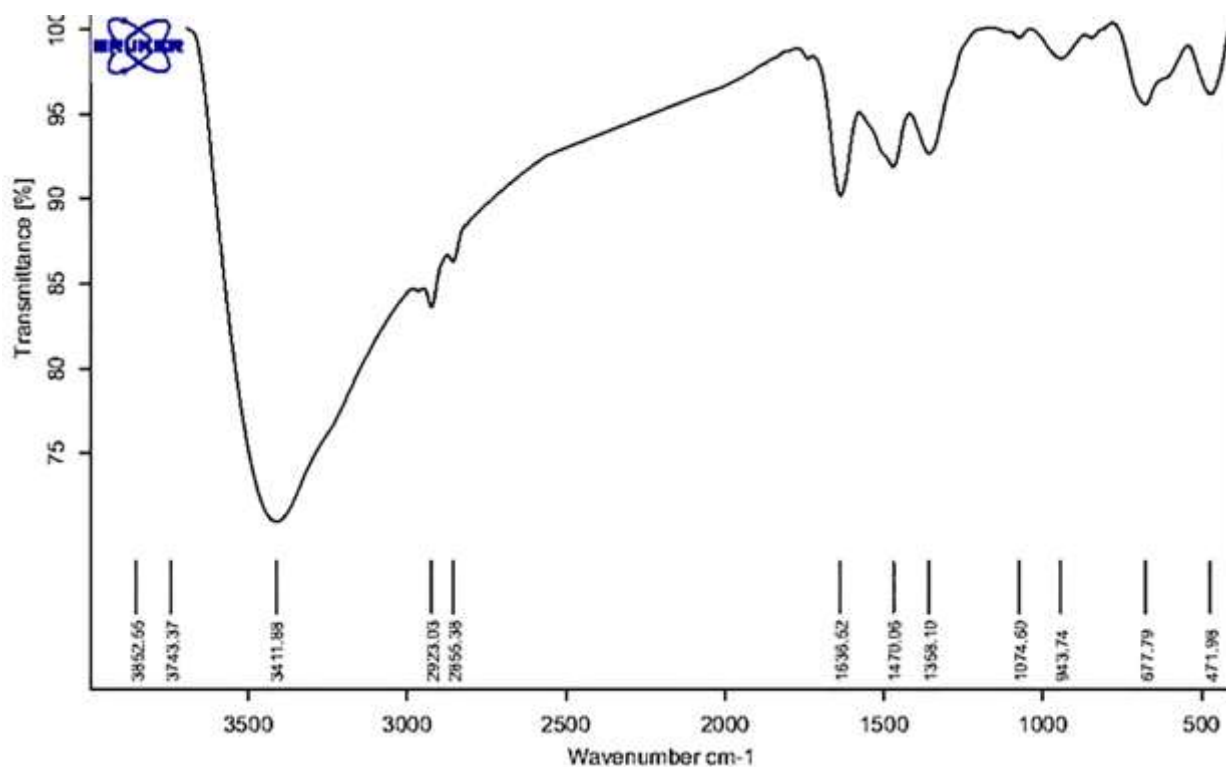


**Fig. 1.** FT-IR spectrum of Fe-Cu binary oxide with a Cu:Fe molar ratio of 1:7

Fig. 2 presents the XRD diffraction pattern of the Fe-Cu binary oxide NPs, in which the crystalline phase of the poorly ordered 2-line ferrihydrite appears at  $35.6^\circ$  and  $61.9^\circ$ . An analysis of this

spectrum approves the synthesized Fe-Cu binary oxide is amorphous and 2-line ferrihydrite-like [3, 27, 44].

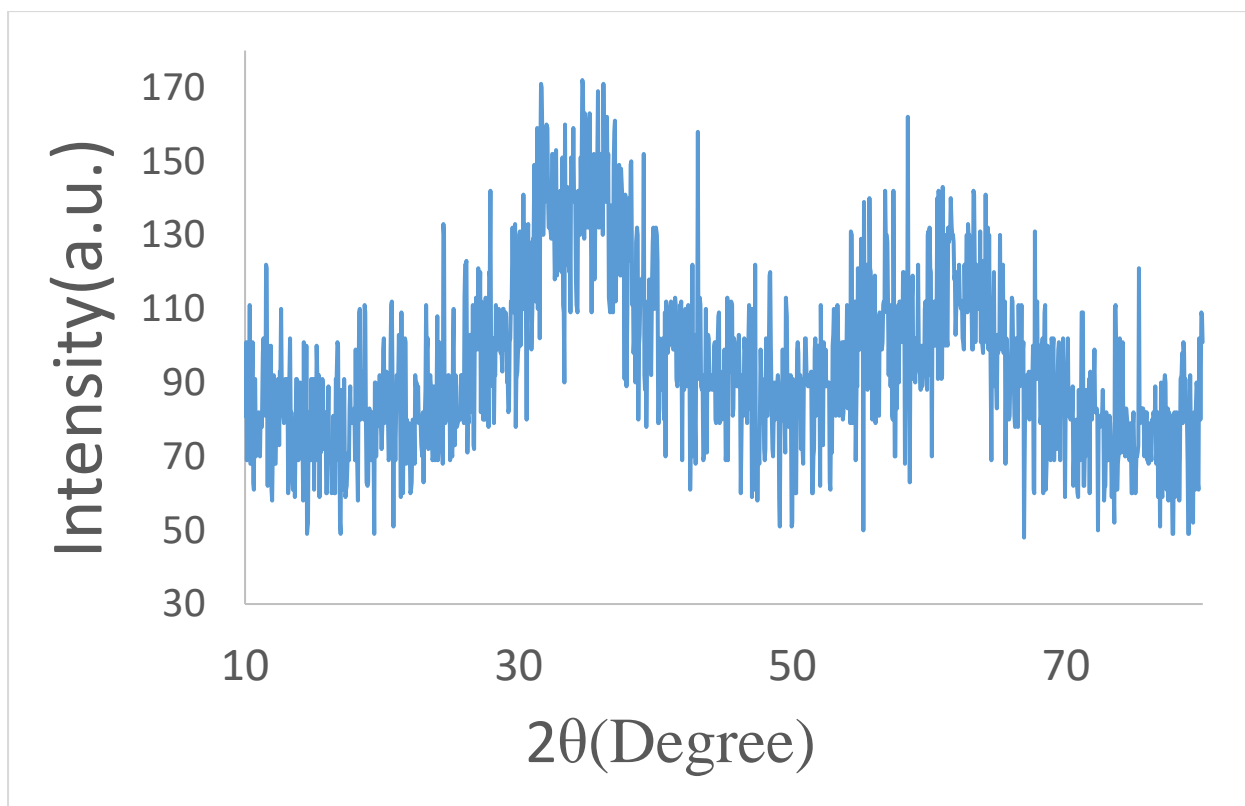


**Fig. 2.** XRD diffractogram of Cu/Fe 1:7 molar ratio of Fe-Cu binary oxide.

Additionally, the surface morphology of Fe-Cu binary oxide was further characterized by SEM, as publicized in Fig. 3. The SEM images of the adsorbent were recorded at two different magnifications with the scale bar of 200 nm (Fig. 3a) and 500 nm (Fig. 3b). The bimetal oxide nanoparticles were roughly spherical in shape and had heterogeneous particle-size distribution. Fig. 4 represents the TEM of Fe-Cu binary oxide with the

scale bars of 100 nm (a) and 75 nm (b) and the size distribution histogram for Fe-Cu binary oxides ( $n = 200$ ,  $n$  is the number of particles) (c). The surface of the Cu-Fe binary oxide was further observed by TEM, and it was found that irregular branching structures surrounded the sphere, and over 80 % of the total count was in the range of 4-10 nm, which demonstrated that the size of the prepared Fe-Cu binary oxide was relatively uniform.

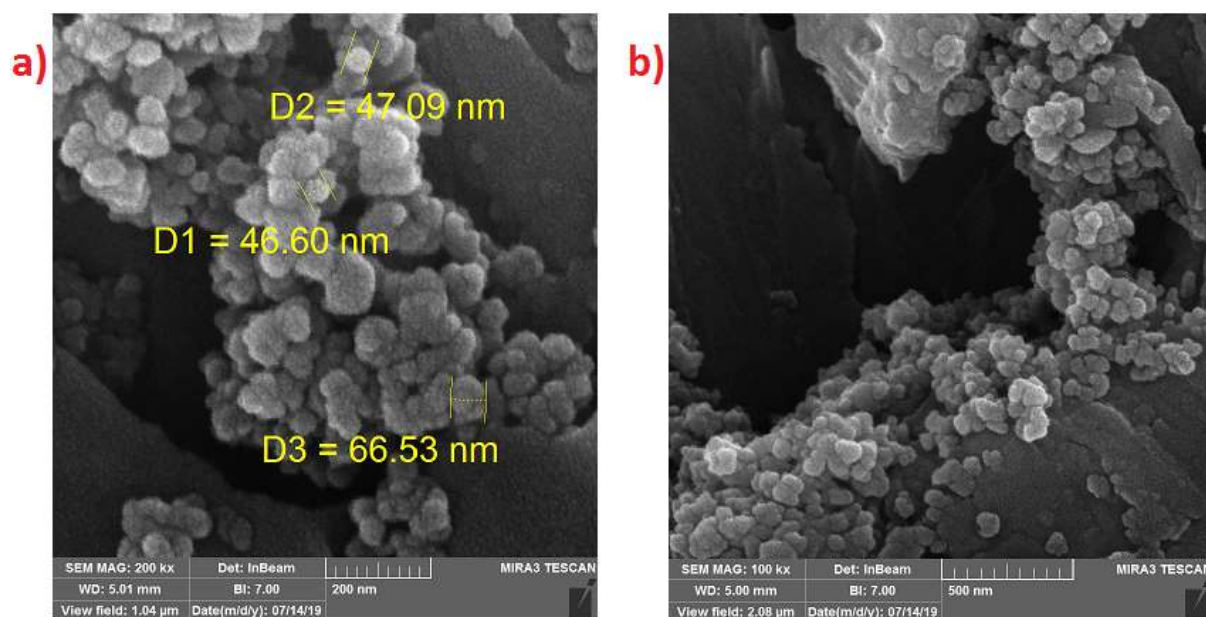


Fig. 3. FE-SEM micrographs of Fe-Cu binary oxide with the scale bars of 200 nm (a) and 500 nm (b)

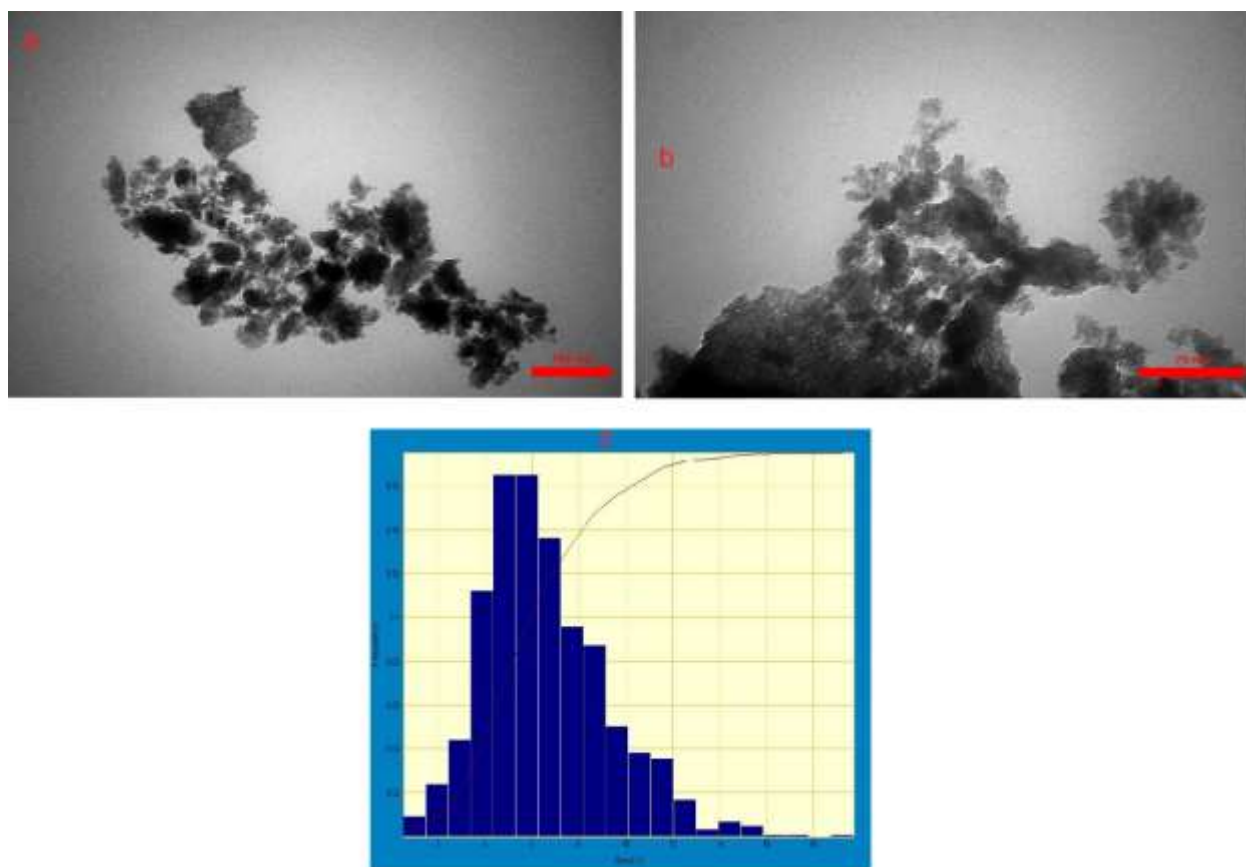
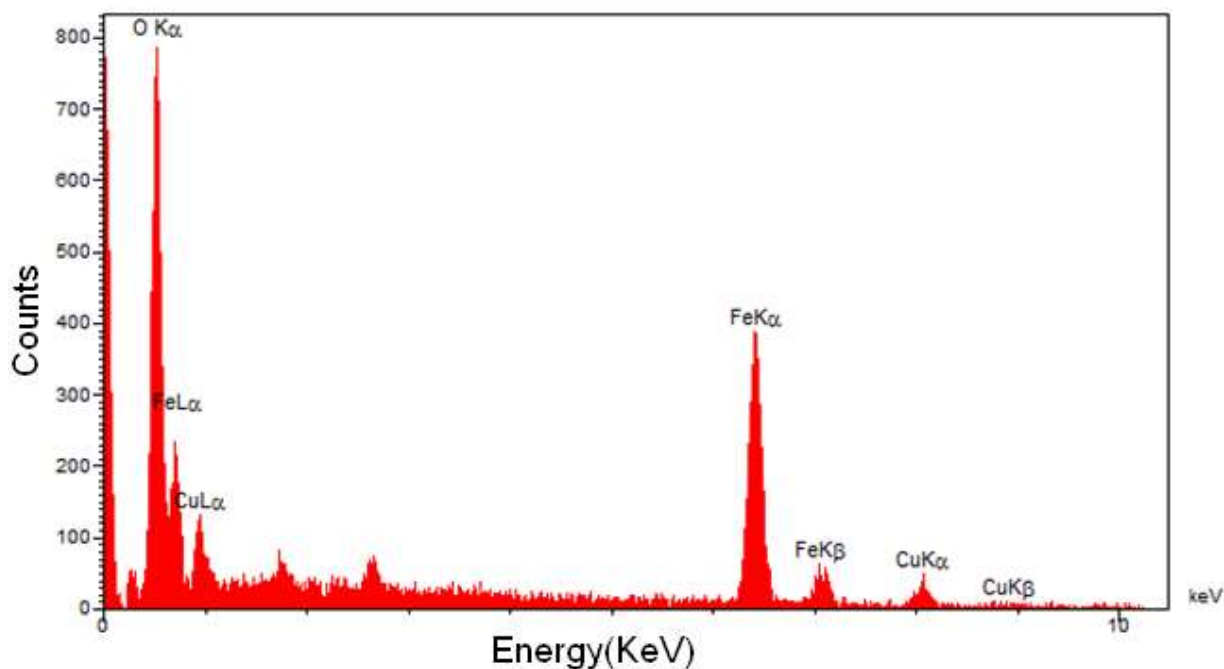


Fig. 4. TEM of Fe-Cu binary oxide with the scale bars of 100 nm (a) and 75 nm (b) and the size distribution histogram for Fe-Cu binary oxides ( $n = 200$ ,  $n$  is the number of particles) (c)

Further confirmation from the structure of the nanomaterials was carried out by EDS analysis (Fig. 5.). In order to observe the kinds of elements in Fe-Cu binary oxide, characteristic peaks containing Fe,

O, and Cu are an indication of the formation of this binary oxide. Besides, another point taken from the EDS analysis is that extra impurity-related peaks were not observed.



**Fig. 5.** EDX spectrum of Fe-Cu binary oxide

The EDX mapping images for Fe-Cu binary oxide are shown in Fig. 5. The analysis of EDS mapping reveals that elements of iron, oxygen, and copper exist in the structure of binary oxide, and their distribution at the bimetal oxide surface is uniform. Moreover, the EDX mapping result repeatedly disproves the presence of any other elemental impurities in the synthesized bimetal oxide. The

magnetic property of as-synthesized Fe-Cu binary oxide NPs determined by vibrating sample magnetometer (VSM) at room temperature. The results of magnetization measurement as a function of applied magnetic field are shown in Fig. 6. It could be seen from the loops that saturation magnetization (MS) of Fe-Cu binary oxide NPs is  $1.5 \text{ emu g}^{-1}$ .

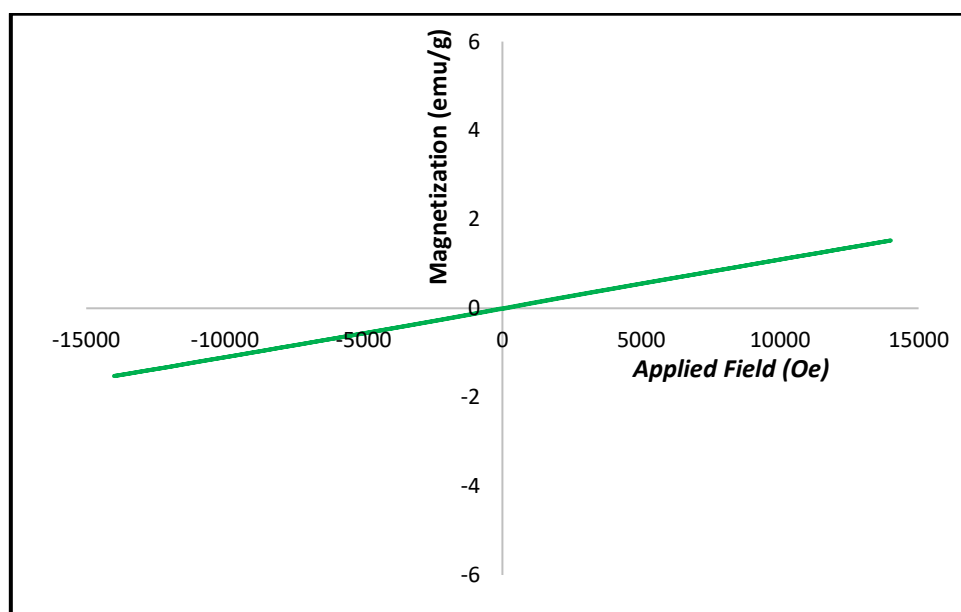


**Fig. 6.** Hysteresis loop of Fe-Cu binary oxide with a Cu/Fe molar ratio of 1:7.

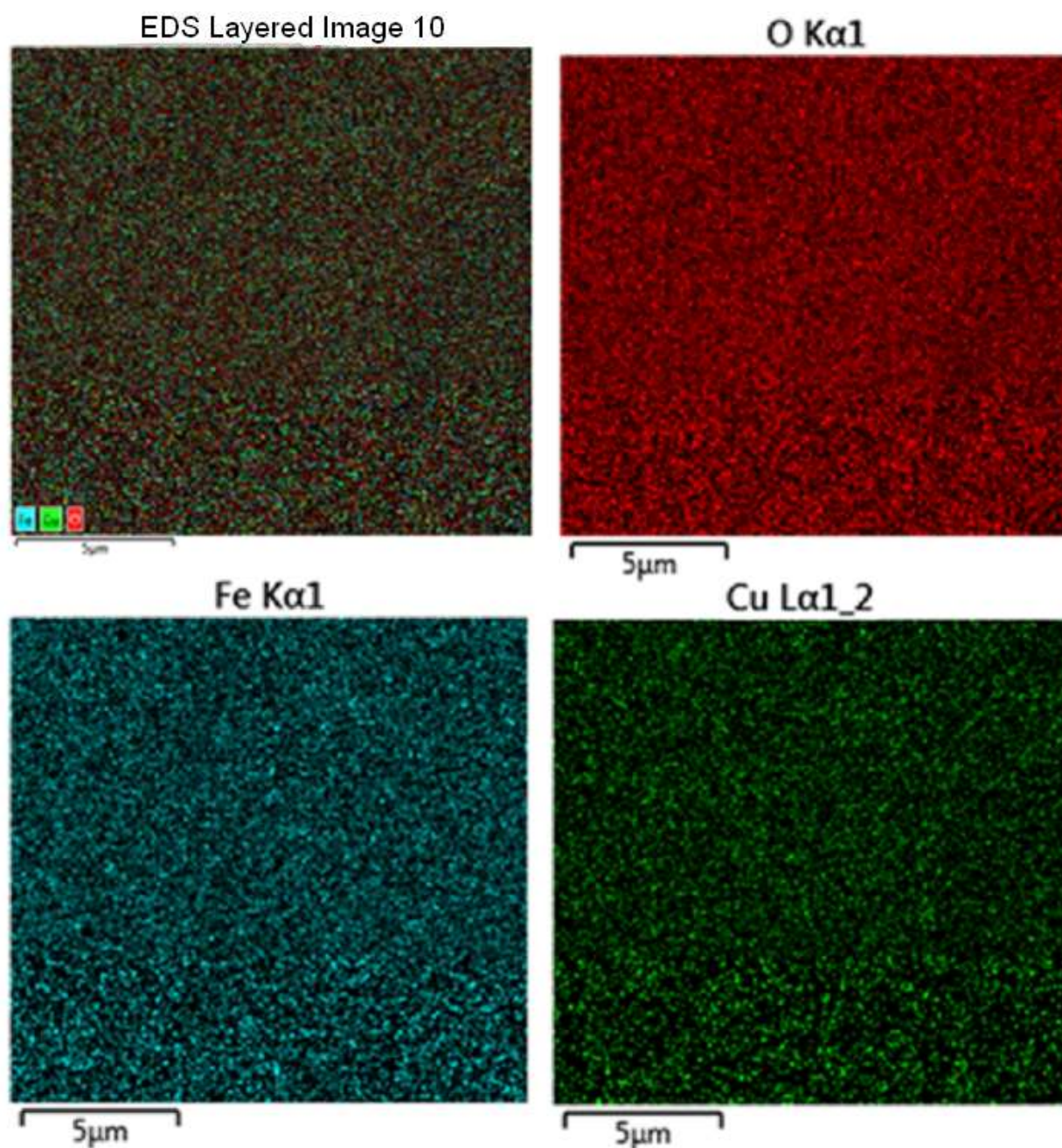


Fig. 7. EDX-MAP of the elements in the structure of Fe-Cu binary oxide

### 3.2. Adsorption of the dyes onto Fe-Cu binary oxide

To evaluate the photocatalytic activity of binary oxide with different Cu:Fe ratio on the acid red 14 (AR14), malachite green (MG), and methyl orange (MO) removal, we set the conditions of analyses variedly.

#### 3.2.1. Influence of Cu:Fe molar ratio on dyes sorption

In binary oxides like Fe-Cu, it has been detected that the Cu:Fe molar ratio is a critical parameter in photocatalytic dye decomposition [33]. To investigate the competitive behavior of the Cu-Fe binary oxide on dye adsorption, we used 15 mgL<sup>-1</sup> photocatalyst dosages<sup>1</sup> at a pH of 7.0 and a temperature of 25 °C for AR14, MO, and MG. The magnetic property of the as-synthesized Fe-Cu binary oxide NPs was determined by vibrating sample magnetometer (VSM) at room temperature.

The results of magnetization measurement, as a function of the applied magnetic field, are shown in Fig. 8. It could be seen from the loops that the saturation magnetization (MS) of the Fe-Cu binary oxide NPs is  $1.5 \text{ emu g}^{-1}$ .

For the competitive adsorption of the same dyes vs. Fe-Cu binary oxides, a series of molar ratios of Cu to Fe 0:1, 1:10, 1:7, 1:5, and 1:0 were employed. The oxides with molar ratios of 1:0 and 0:1 were named as CuO and FeOOH, respectively. Fig. 9 displays the influence of Cu:Fe molar ratios on dye removals as a function of dye concentrations. When the initial AR14 concentrations were  $\leq 50 \text{ mgL}^{-1}$ , ~91% AR14 was removed by binary oxide with Cu:Fe molar ratio of 1:7. Subsequently, similar batch equilibrium experiments were conducted for the removal of the

MO, and the proposed procedure was achieved. The maximum removal efficiency (~ 89%) occurred at the same molar ratio; then, when the molar ratio led to an increase in the amount of copper, the removal percentage decreased dramatically. With the addition of binary oxides with Cu:Fe molar ratios of 0:1, 1:10, and 1:7, as the photocatalyst, the MG removal efficiency increased by 25%, 49%, and 87%, respectively. The Cu:Fe 1:7 molar ratio of Fe-Cu binary oxide with the as feasible sorbent was used in this experiment. This sorbent was examined in the photocatalyst reaction test section in detail. It is noteworthy that all three dye removal efficiencies by this binary oxide were superior to the monometallic iron and copper catalysts.

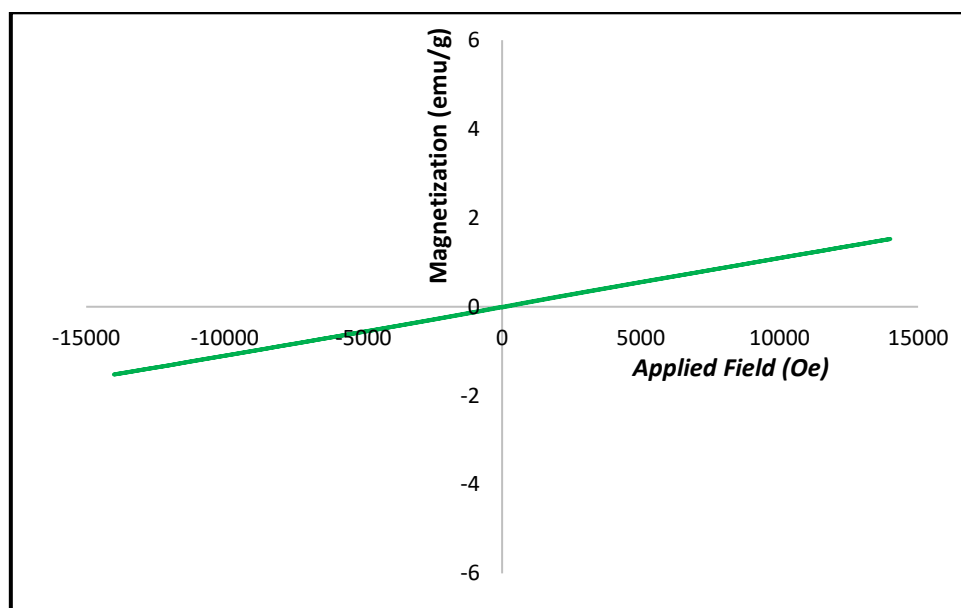


**Fig. 8.** Hysteresis loop of Fe-Cu binary oxide with a Cu/Fe molar ratio of 1:7

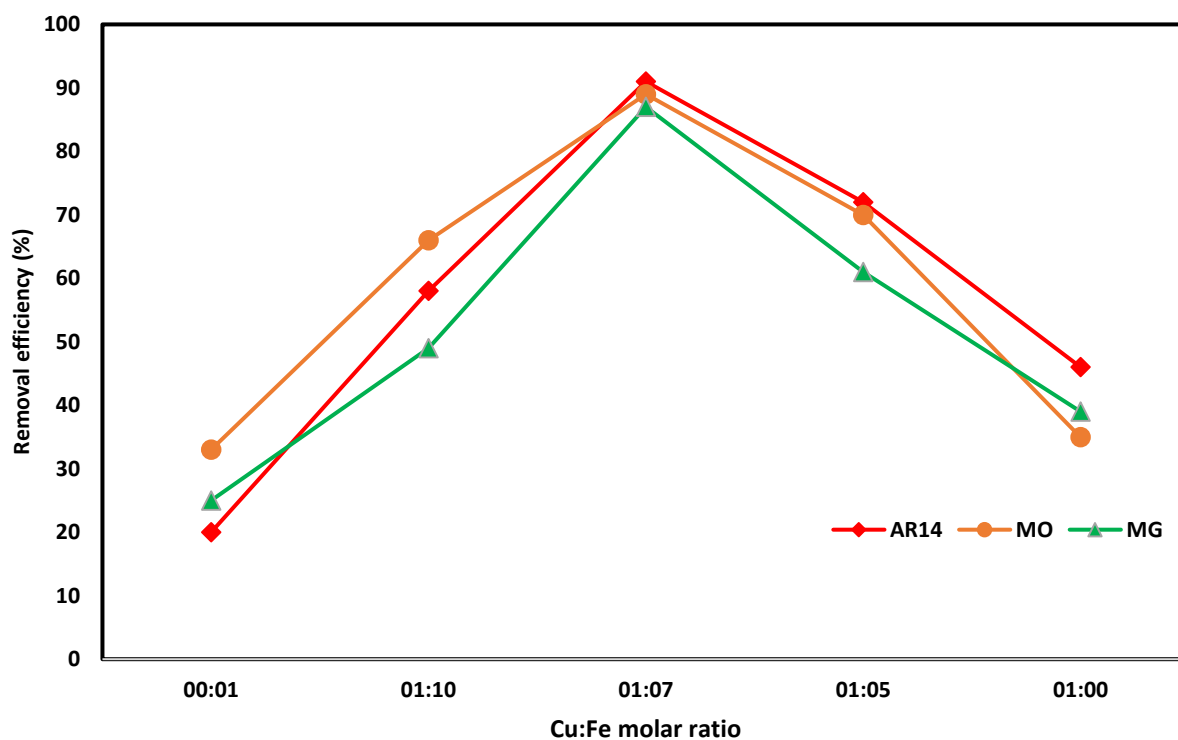


**Fig. 9.** Effect of Cu:Fe molar ratio on dyes adsorption by Fe-Cu binary oxide; Initial dye concentration:  $50 \text{ mgL}^{-1}$ , adsorbent dose:  $15 \text{ mgL}^{-1}$ , pH:  $7.0 \pm 0.1$ , agitation speed: 200 rpm, and temperature:  $25 \pm 1^\circ\text{C}$

### 3.2.2. Influence of initial solution pH on dyes sorption

One of the essential controlling parameters in the adsorption process is the pH of the solution for the reason that it impacts both surface binding site and aqueous charge distribution of the sorbent [4]. Since the degradation of dyes in colored effluents depends on the pH range, the comparative experiments with the optimized molar ratio of the binary oxide were performed at a pH range of 2.0-13.0 on three reactive dyes. Initial dye concentration (50 ppm) and temperature ( $25^\circ\text{C}$ ) were reserved constant. Fig. 10 shows that the removal percentage of the anionic AR14 is preserved above 94% at the pH of 2.0. With increases in the pH from 3.0 to 13.0, the removal percentage slowly reduces to less than 45% at 1 h. The hydrolysis reaction that happens between the metal oxide and water causes the generation of surface hydroxyl groups [45]. The metal oxides that possess surface hydroxyl groups are presented as the predominant and active adsorption sites for the

adsorption of dyes from water. Because of the hydroxyl groups located on the surface of NPs, the Fe-Cu binary oxide NPs have positive charges at acidic pH values.

Consequently, in the acidic pH range, the availability of negatively charged AR14 to the hydroxyl active site increased. This is especially visible when the pH had no remarkable effect, over a wide pH range 6.0-13.0, on the removal of MO on the Fe-Cu binary oxide NPs. The removal efficiency of MO remained above 90% in the pH of 2. Therefore, Fig. 10 shows that the removal of both dyes was pH-dependent, and the maximum uptake of the dye occurred at the pH of 2. The results reveal that the decolorization of the cationic MG on the Fe-Cu binary oxide is reinforced as pH increases from 8.0 to 13.0 and decreased at pH below 7 from the initial concentration of the dye solutions. These observations related to the positive adsorbent surface charge of nanoparticles. The percentage comparison of dye removals by the selected binary

oxide from the aqueous solutions at acidic, neutral, and alkaline pH (94% at the pH of 2.0 for the anionic acid red 14, 90% at the pH of 2.0 for the anionic

methyl orange, and 94.0 at the pH of 8.0 for cationic malachite green) gave more quantitative insight of the reaction.

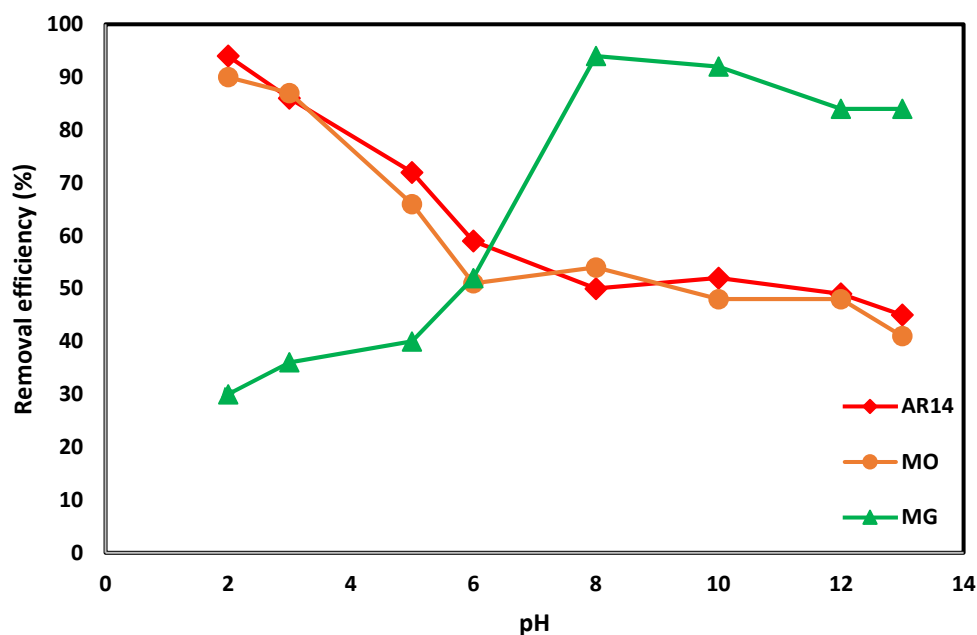


**Fig. 10.** Effects of solution pH on dyes adsorption by Fe-Cu binary oxide; Initial dye concentration: 50 ppm, adsorbent dose: 15 mgL<sup>-1</sup>, agitation speed: 200 rpm, and temperature: 25 ± 1°C.

### 3.2.3. Influence of adsorbent dosage on dyes sorption

We considered the adsorption capacity of the adsorbent by setting the adsorbent quantity in the range of 0-35 mgL<sup>-1</sup> for all dyes (Fig. 11). According to this diagram, the adsorption percentage of AR14 and MO starts to increase as the adsorbent quantity rises to 15 mg. That is because of the accessibility of more adsorbent surfaces for these dyes to be

adsorbed. Then, dyes sorption decreases with a further increase in adsorbent dosage, and it remains at a constant value. Fig. 10 shows increasing the amount of adsorbent by removal efficiencies of the MG. It revealed that over 95% of adsorption was gained by 20 mg of the sorbent compound. The considerable change was not shown in dye removal efficiency. It should be mentioned that the number of active sites increases by as dosage increases.

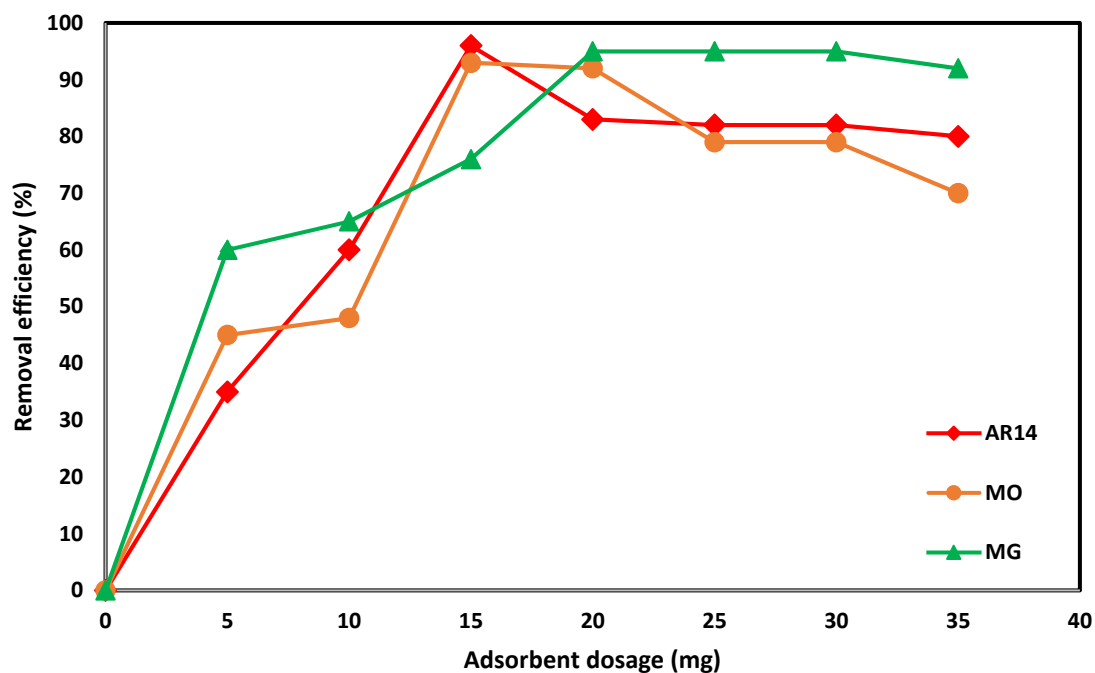


Fig. 11. Effects of adsorbent dosage on dyes adsorption by Fe-Cu binary oxide; Initial dye concentration: 50 mgL<sup>-1</sup>, pH of dye solution: 7, agitation speed: 200 rpm, and temperature: 25 ± 1°C.

### 3.2.4. Catalytic tests of Fe-Cu binary oxide with the Cu:Fe molar ratio of 1:7 as a photocatalyst

#### 3.2.4.1. Spectral and UV changes of AR14 in the presence of Fe-Cu binary oxide

The results of changes in the absorption spectra of AR14 during photocatalytic decolorization triggered by the Fe-Cu binary oxide are shown in Fig. 12. The decrease in the absorption of AR14 with prolonging irradiation time at 508 nm assumes the decolorization of dye. The changes in the absorption spectra of MO during photocatalytic decolorization

resultant from the use of the Fe-Cu binary oxide have been estimated. The absorption of the visible band at 465 nm decreased as the irradiation time increased. The absorbance of MG solutions during the process at initial and after 180 min irradiation time was investigated. The spectrum of MG in the visible region shows a strong band with a maximum of 619 nm. The decrease in absorption peaks of MG at this band indicates a quick decolorization of the dye. A complete discoloration of dye was observed after 180 min under optimal conditions.

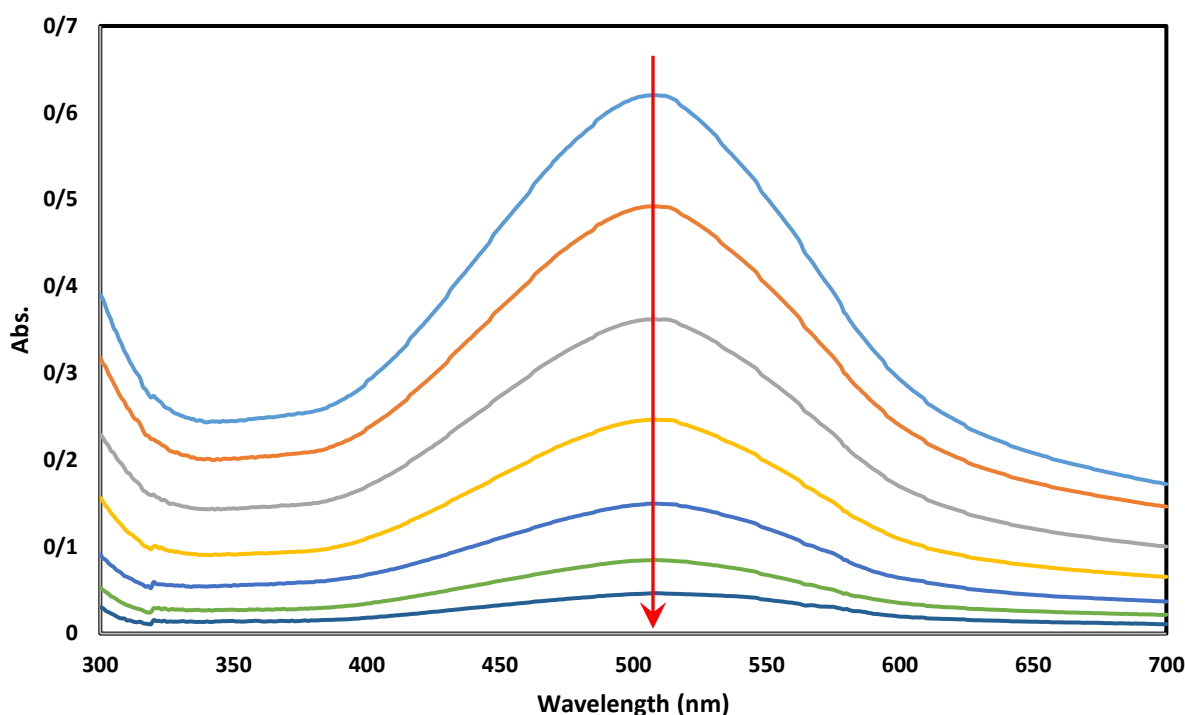


Fig. 12. UV- vis spectral changes of AR14, recorded during the photocatalytic decolorization in the presence of Fe-Cu binary oxide; Adsorbent dosage: 15 mg, initial dye concentration: 50 ppm, pH of dye solution: 7, agitation speed: 200 rpm, and temperature:  $25 \pm 1^\circ\text{C}$ .

### 3.2.4.2. Kinetics of photocatalytic degradation of AR14, MO, and MG

Fig. 11 displays the photocatalytic properties of the Fe-Cu binary oxide with the Cu:Fe molar ratio of 1:7 in dye solution under  $25^\circ\text{C}$  with an irradiation time of 180 min and a pH of 7. The pH was kept the identical amount for comparative experiments. These conditions are the same for the other two color removal experiments. It can be seen that AR14 was slightly stable in the absence of a photocatalyst. With the addition of photocatalyst, the AR14 removal efficiency increased by 94%. Fig. 14 shows the color removal efficiency of the MO solution as a function of initial concentration. Hence the effect of MO concentration was investigated at different initial concentrations in the range of  $0\text{--}1\text{ mgL}^{-1}$ . As shown in Fig. 12 decolorization percent decreases as the initial concentration of MO increases. It is noteworthy that the MO removal efficiency by the mentioned photocatalyst was superior to the without catalyst experiment. Fig. 14 shows the results of MG

removal with and without the binary oxide photocatalyst. The medium self-decomposition activity for MG (50%) under UV irradiation was obtained in the photocatalyst free system.

Moreover, decomposition percent of MG on Fe-Cu binary oxide was 95%. The plot  $\ln(C_0/C)$  versus irradiation time for AR14, MO, and MG was linear, suggesting that the photocatalytic reaction approximately followed the pseudo-first-order kinetics. The number of the rate constants was estimated from the slope of the  $\ln(C_0/C)$  versus irradiation time plot in the optimized conditions. As shown in Fig. 13, 14, and 15, the rate constant of AR14, MO, and MG after 3 h is  $0.0147$ ,  $0.0058$ , and  $0.0253\text{ min}^{-1}$ , respectively. The MO degradation occurred somewhat in the presence of the Fe-Cu binary oxide. In contrast, the reaction rate for MG was significantly improved with a degradation rate constant of about  $0.0253\text{ min}^{-1}$ , which is larger than that of AR14 ( $0.0147\text{ min}^{-1}$ ) and MO ( $0.0058\text{ min}^{-1}$ ).

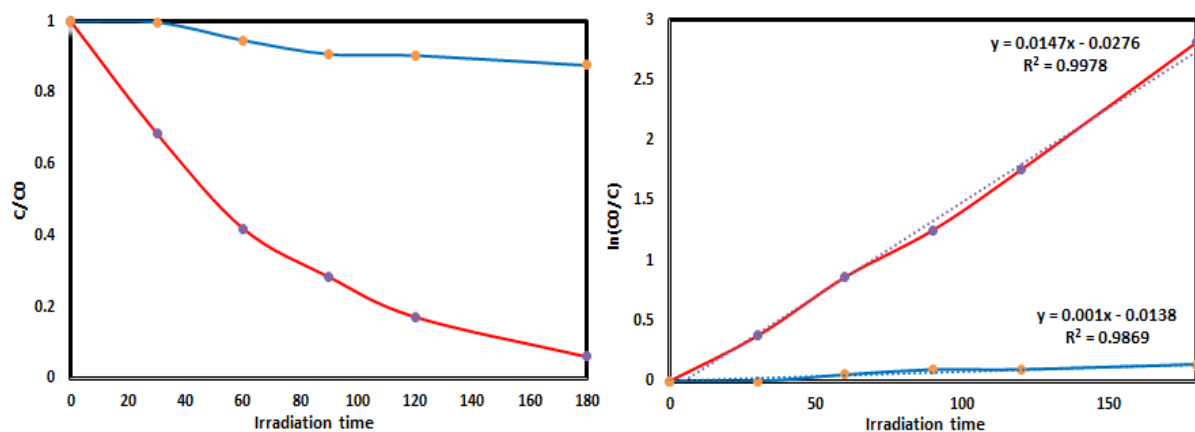


Fig. 13. The removal efficiency of AR14 with and without photocatalyst during the reaction in 180 min, at pH of 7.0 with  $1 \text{ gL}^{-1}$  catalyst dosage, 50 ppm AR14,  $25^\circ\text{C}$

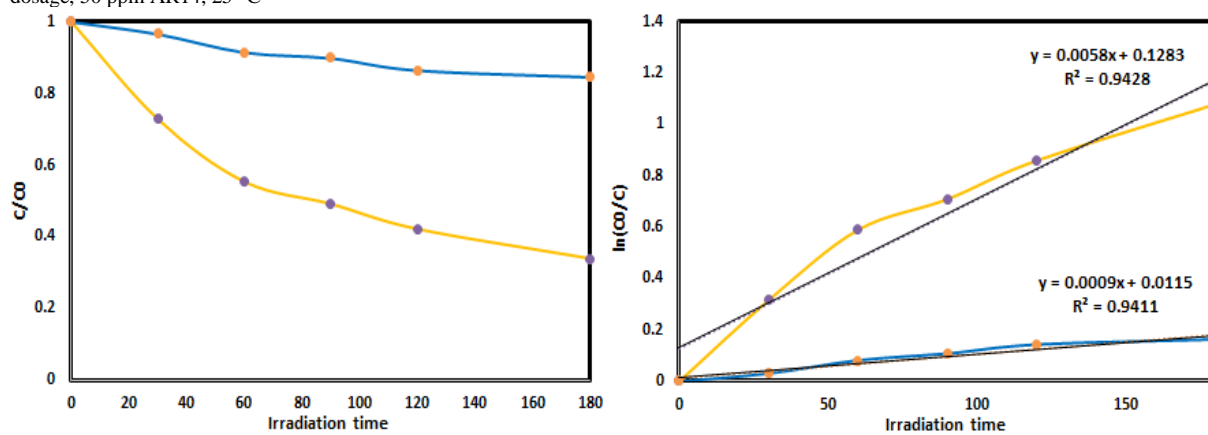


Fig. 14. The removal efficiency of MO with and without photocatalyst during the reaction in 180 min, at pH of 7.0 with  $1 \text{ gL}^{-1}$  catalyst dosage, 50 ppm MO,  $25^\circ\text{C}$

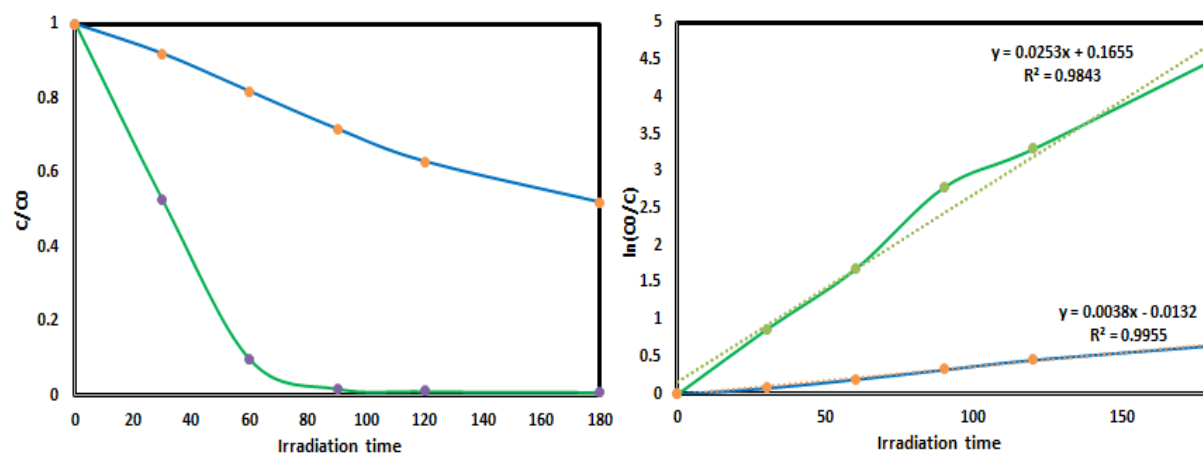


Fig. 15. The removal efficiency of MG with and without photocatalyst during the reaction in 180 min, at pH of 7.0 with  $1 \text{ gL}^{-1}$  catalyst dosage, 50 ppm MG,  $25^\circ\text{C}$

#### 4. Conclusions

In conclusion, a series of iron-copper binary oxide nanoparticles with different Cu:Fe ratios were prepared from inexpensive precursors by a simple co-precipitation method. The removal of Acid Red 14, Methyl Orange, and Malachite Green by these

nanostructures was studied in a batch reactor. The UV irradiation was used for the exploration of the effect of different operational parameters such as Cu:Fe molar ratio, pH, and sorbent dosage. The photocatalytic results exhibited that the dye removal activity depended highly upon the Cu:Fe ratio. 1:7 is

the optimum molar ratio for the attainment of the best dye removal activity. Various techniques were used for the characterization of the synthetic Fe-Cu binary oxide with a Cu:Fe molar ratio of 1:7. Decolorization of dyes follows a pseudo-first-order kinetic, and the nanostructure of binary oxides has an imperative role in the removal of dyes. Under the

### References

- [1] Ghaedi M, Ghaedi A, Hossainpour M, Ansari A, Habibi M, Asghari A, *Journal of Industrial and Engineering Chemistry*, **20**(2014) 1641.
- [2] Iram M, Guo C, Guan Y, Ishfaq A, Liu H, *Journal of hazardous materials*, **181**(2010) 1039.
- [3] Couto SR, *Biotechnology advances*, **27**(2009) 227.
- [4] Alver E, Metin AÜ, *Chemical Engineering Journal*, **200**(2012) 59.
- [5] Moghaddam SS, Moghaddam MA, Arami M, *Journal of hazardous materials*, **175**(2010) 651.
- [6] Chu W, *Water Research*, **35**(2001) 3147.
- [7] Mondal S, *Environmental Engineering Science*, **25**(2008) 383.
- [8] Ergas SJ, Therriault BM, Reckhow DA, *Journal of Environmental engineering*, **132**(2006) 315.
- [9] De Vreese I, Van der Bruggen B, *Dyes and pigments*, **74**(2007) 313.
- [10] Gupta V, *Journal of environmental management*, **90**(2009) 2313.
- [11] Vakili M, Rafatullah M, Salamatinia B, Abdullah AZ, Ibrahim MH, et al, *Carbohydrate polymers*, **113**(2014) 115.
- [12] Crini G, *Bioresource technology*, **97**(2006) 1061.
- [13] Kango S, Kalia S, Celli A, Njuguna J, Habibi Y, Kumar R, *Progress in Polymer Science*, **38**(2013) 1232.
- [14] Zhang D, Zhou C, Sun Z, Wu L-Z, Tung C-H, Zhang T, *Nanoscale*, **4**(2012) 6244.
- [15] Li L, Xiao J, Liu P, Yang G, *Scientific reports*, **5**(2015) 9028
- [16] Salehi R, Arami M, Mahmoodi NM, Bahrami H, Khorramfar S, *Colloids and Surfaces B: Biointerfaces*, **80**(2010) 86.
- [17] Mohamed MM, Othman I, Mohamed R, *Journal of Photochemistry and Photobiology A: Chemistry*, **191**(2007) 153.
- [18] Afkhami A, Moosavi R, *Journal of Hazardous Materials*, **174**(2010) 398.
- [19] Reddy DHK, Lee S-M, *Advances in colloid and interface science*, **201**(2013) 68.
- [20] Zinatloo-Ajabshir S, Morassaei MS, Amiri O, Salavati-Niasari MJCI, **46**(2020) 6095.
- [21] Mortazavi-Derazkola S, Zinatloo-Ajabshir S, Salavati-Niasari MJAPT, **28**(2017) 747.
- [22] Zinatloo-Ajabshir S, Salehi Z, Salavati-Niasari MJJoCP, **192**(2018) 678.
- [23] Zhang Y, Yang M, Dou X-M, He H, Wang D-S, *Environmental Science & Technology*, **39**(2005) 7246.
- [24] Zhang G, Qu J, Liu H, Liu R, Wu R, *Water research*, **41**(2007) 1921.

- [25] Gupta K, Ghosh UC, Journal of hazardous materials, **161**(2009) 884.
- [26] Liu S, Kang S, Wang G, Zhao H, Cai W, Journal of colloid and interface science, **458**(2015) 94.
- [27] Ren Z, Zhang G, Chen JP, Journal of colloid and interface science, **358**(2011) 230.
- [28] Yang M, He J, Journal of colloid and interface science, **355**(2011) 15.
- [29] Nekouei F, Nekouei S, Tyagi I, Gupta VK, Journal of Molecular Liquids, **201**(2015) 124.
- [30] Zhang G, Ren Z, Zhang X, Chen J, Water Research, **47**(2013) 4022.
- [31] Li G, Gao S, Zhang G, Zhang X, Chemical Engineering Journal, **235**(2014) 124.
- [32] Tofik A, Taddesse AM, Tesfahun K, Girma GJJoece, **4**(2016) 2458.
- [33] Li Y, Hu X, Ren B, Yue J, Yang WJD, Treatment W, **57**(2016) 26461.
- [34] Jacukowicz-Sobala I, Ociński D, Mazur P, Stanisławska E, Kociołek-Balawejder EJJoHM, 2020) 122527
- [35] Gilanizadeh M, Zeynizadeh B, Research on Chemical Intermediates, **44**(2018) 6053.
- [36] Casillas JE, Campa-Molina J, Tzompantzi F, Carbajal Arízaga GG, López-Gaona A, et al, **13**(2020) 1345
- [37] Tuan TNJVJoS, Technology, **56**(2018) 1.
- [38] Lakhera SK, Venkataramana R, Watts A, Anpo M, Neppolian BJRoCI, **43**(2017) 5091.
- [39] Hafeez HY, Lakhera SK, 2018)
- [40] Di G, Zhu Z, Zhang H, Zhu J, Lu H, et al, **328**(2017) 141.
- [41] Chen S, Li M, Yang S, Li X, Zhang SJASS, **492**(2019) 571.
- [42] Ozturk B, Soyulu GSPJCI, **42**(2016) 11184.
- [43] Lu K, Wang T, Zhai L, Wu W, Dong S, et al, **539**(2019) 553.
- [44] Schwertmann U, Cornell RM, *Iron oxides in the laboratory: preparation and characterization*. (2008). John Wiley & Sons
- [45] Wachs IEJCT, **27**(1996) 437.